

Optical reconstruction of collective density matrix of qutrit

Marek Kopciuch¹ and Szymon Pustelny¹

¹*Institute of Physics, Jagiellonian University in Kraków, Łojasiewicza 11, 30-348 Kraków, Poland*
(Dated: March 21, 2022)

Reconstruction of a quantum state is of prime importance for quantum-information science. Specifically, means of efficient determination of a state of atoms of room-temperature vapor may enable applications in quantum computations and cryptography. To step toward such applications, here we present a method of reconstruction of a collective density matrix of an atomic ensemble, consisting of atoms with an $F = 1$ ground state. Such a long-lived state is often encountered in real systems (e.g., potassium, sodium, rubidium) and hence may be practically utilized. Our theoretical treatment enables derivation of explicit formulas relating optical signals (polarization rotation and ellipticity change) with specific density-matrix elements. The analysis are supported with numerical simulations, which allows to evaluate fidelity and robustness of the algorithm. The tests show that our algorithm allows to obtain the fidelity exceeded 0.95 even at noisy environment and/or significant atomic manipulation imperfections.

Introduction – One of the most important challenges of quantum information science is reconstruction of an unknown quantum state [1–5]. The reconstruction requires measurements of different noncommuting observables on a set of systems occupying the same quantum state. Unfortunately, due to the no-cloning theorem [6], preparation of identical copies of a single quantum state is impossible. Utilization of a macroscopic system, composed of a large number of particles and described by a collective quantum state, enables measurements over many elements at the same time [5, 7]. Interpretation of such reconstruction is straightforward in media composed of particles in an identical quantum state. A specific example of such systems is the Bose-Einstein condensate, where all atoms reside in the same quantum state [3]. The situation is different in room-temperature atomic vapors, where inhomogeneous transition broadening leads to velocity-dependent interaction with external fields (the Doppler effect) and, as a result, atoms in various quantum states of simultaneously present in the medium. Nonetheless, even in such a case, there are distinct examples, where atoms may be considered as occupying the same quantum state. A specific example of such a situation is an atomic vapor contained in a paraffin-coated cell, where atoms freely travel between container walls, but their polarization is preserved in the wall collisions [8–10]. Thereby the atoms interact with light multiply times, experiencing different Doppler shifts before finally relaxing. As a result, interaction is averaged over an entire cell volume [8, 9]). While in reality the system’s state is a statistical average over quantum states of its microscopic elements, it still possesses many features of a quantum state, revealing numerous quantum properties (shot noise [11, 12], squeezing [11], entanglement [13], etc.), hence being interesting from the point of view of quantum-state tomography.

In this work, we present an approach to reconstruct the collective density matrix [14, 15] of atoms in atomic ensemble based on continuous weak measure-

ments [7, 15, 16]. In weak measurements, the system under investigation is weakly perturbed during probing, hence the attainable information is limited. This fact can be regained by performing measurements at many atoms at the same time. This approach has been already implemented in quantum state tomography of cold atomic system (see, for example, Ref. [7]), however, in contrast to the works, our approach is described in a semiclassical picture, in which incident light is purely classical field, which is sufficient and conventional way of describing light-atom interaction in room temperature regime [17]. As the overall evolution of such a system is complicated, we perform a series of approximations suitable for alkali vapors at room temperature. It allows us to describe analytically the evolution of a system and derive formula relating polarization rotation and ellipticity change with quantum properties of atoms. We demonstrate application of the approach for reconstruction of a full density matrix of a three-level system (qutrit) formed within magnetic sublevels of long-lived ground state [10, 18]. Information about quantum state is obtained based on measurements of properties of light traversing the system at nonzero magnetic field. The technique is implemented for reconstruction of both pure and mixed states, and its precision and robustness against different limitations (noise and uncertainties) is being investigated.

Relation between observables and quantum-state properties – Optical tomography of a quantum state is based on measurements of specific properties of light propagating through a medium consisting of atoms whose quantum state one wants to reconstruct. Particular examples of observables providing such information are: the polarization angle α and the degree of ellipticity ϵ . In the Supplemental Information (SI), the relations of the two observables with the density-matrix elements, characterizing the atoms of the $F = 1$ ground state and $F' = 0$ excited state, where F and F' denote the total angular momentum in the ground- and excited state, respectively, are derived. While the formulas in SI are given for any

polarization of light propagating along the z direction, here, we limit ourselves to the case of x -polarized light. This allows us to write the spatial derivative of polarization rotation $\partial_z \alpha$ and the ellipticity $\partial_z \epsilon$ as

$$\partial_z \alpha - i \partial_z \epsilon = -\chi(\tilde{\rho}_{-10'} + \tilde{\rho}_{10'}), \quad (1)$$

where $\tilde{\rho}_{mn'}$ is the amplitude of the optical coherence between the ground state m and the excited state n' ($\tilde{\rho}_{mn'}$ is given the rotating-wave approximation) and $\chi = \omega N_{at} \langle 1 | \hat{\mathbf{d}}^{(F)} | 0' \rangle / (\sqrt{6} \epsilon_0 E_0 c)$ is a constant determined by the light frequency ω and amplitude E_0 , and the atomic number density N_{at} . The reduced dipole-matrix element $\langle 1 | \hat{\mathbf{d}}^{(F)} | 0' \rangle$ is calculated in the F manifold (relation between the J and F basis is discussed in SI). It should be noted that precise knowledge of χ is of a crucial importance for the quantum-state tomography.

Evolution of optical coherence of atoms subjected to the magnetic field B_z and interacting with x -polarized light, detuned from the optical transition by Δ , is derived in SI. For the current discussion, we simplify the relations by noting that (1) the ground-state relaxation rate γ is typically several orders of magnitude smaller than the excited-state relaxation rate Γ , $\Gamma \gg \gamma$, and (2) the Larmor frequency Ω_L is small compared to the detuning Δ , $\Delta \gg \Omega_L$. This allows us to simplify the equation for time evolution of the optical-coherence amplitude

$$\dot{\tilde{\rho}}_{\pm 10'} = -\tilde{\rho}_{\pm 10'} \left(\frac{\Gamma}{2} + i\Delta \right) \pm \frac{i\Omega_R}{2\sqrt{6}} (\tilde{\rho}_{\pm 1 \pm 1} - \tilde{\rho}_{0'0'} - \tilde{\rho}_{\pm 1 \mp 1}), \quad (2)$$

where Ω_R is the Rabi frequency, $\tilde{\rho}_{mm}$ is population of the ground-state magnetic sublevel m and $\tilde{\rho}_{mn}$ is the ground-state Zeeman coherence between the m and n sublevels.

Taking a time derivative of Eq. (1) and combining it with Eq. (2) allows us to relate the time-dependent polarization rotation and ellipticity change with the density matrix elements

$$\dot{\partial}_z \alpha = \frac{\Gamma}{2} \partial_z \alpha - \Delta \partial_z \epsilon + \frac{\Omega_R \chi}{2\sqrt{6}} \text{Im} \{ \kappa \}, \quad (3a)$$

$$\dot{\partial}_z \epsilon = \frac{\Gamma}{2} \partial_z \epsilon + \Delta \partial_z \alpha + \frac{\Omega_R \chi}{2\sqrt{6}} \text{Re} \{ \kappa \}, \quad (3b)$$

where $\kappa = \tilde{\rho}_{11} - \tilde{\rho}_{-1-1} + \tilde{\rho}_{-11} - \tilde{\rho}_{1-1}$. The ground-state population ρ_{mm} and coherences ρ_{mn} may be calculated using the Liouville equations (see SI). Assuming weak probe light, the terms proportional to Ω_R^2 and hence the excited-state population $\rho_{0'0'}$, can be neglected, which allows to solve the differential equation and write the time-dependent density matrix elements as

$$\tilde{\rho}_{11}(t) - \tilde{\rho}_{-1-1}(t) = \left(\tilde{\rho}_{11}^{(0)} - \tilde{\rho}_{-1-1}^{(0)} \right) e^{-\gamma t}, \quad (4a)$$

$$\tilde{\rho}_{1-1}(t) = \tilde{\rho}_{-1-1}^{(0)} e^{-\gamma t} e^{-2i\Omega_L t}, \quad (4b)$$

where superscript (0) indicates the density-matrix element prior to probing. Substituting Eqs. (4) into κ and

taking real and imaginary parts of the quantity enable solving Eqs. (3). The system has several time scales related to different processes. Specifically, we exclusively focus on slowly evolving terms (evolution time-scale on order of $1/\Omega_L$), neglecting transient effects, typically occurring at the time scale $1/\Gamma$. It allows us to write polarization rotation and ellipticity change in a compact form

$$\partial_z \alpha = \zeta e^{-\gamma t} \{ \Gamma [A \sin(2\Omega_L t) - B \cos(2\Omega_L t)] + C \Delta \} \quad (5a)$$

$$\partial_z \epsilon = \zeta e^{-\gamma t} \left\{ 2\Delta [A \sin(2\Omega_L t) - B \cos(2\Omega_L t)] - C \frac{\Gamma}{2} \right\} \quad (5b)$$

where $\zeta = 2\chi\Omega_R / [\sqrt{6}(\Gamma^2 + 4\Delta^2)]$, $A + iB = \tilde{\rho}_{1-1}^{(0)}$, and $C = \tilde{\rho}_{-1-1}^{(0)} - \tilde{\rho}_{11}^{(0)}$.

As shown in Eqs. (5), the polarization rotation $\partial_z \alpha$ or ellipticity change $\partial_z \epsilon$ yields information about the ground-state density matrix. Specifically, the oscillating component of the signal is associated with the Zeeman coherence, while the nonoscillating component is proportional to the population difference between the $m = \pm 1$ sublevels. Unfortunately, the accessible information is limited as (1) the signals depend on the population difference (i.e., not on population themselves) and (2) there is no access to population or coherence associated with the $m = 0$ ground-state sublevel. To determine these remaining density-matrix elements we introduce rotations, which mix population and coherences of various magnetic sublevels. Here, we implement the rotations by application of pulses of static magnetic fields. Assuming that the pulses rotate the state around the z axis by φ and around the y axis by ϑ and the pulse lengths are negligibly short, the transformed density matrix is given by

$$\tilde{\rho}^\circledast = \hat{\mathcal{D}}(0, \vartheta, \varphi) \tilde{\rho}^{(0)} \hat{\mathcal{D}}^\dagger(0, \vartheta, \varphi). \quad (6)$$

where $\hat{\mathcal{D}}$ is the quantum-mechanical rotation operator. Using Eq. (6), one can calculate the dependence of specific density-matrix elements on the rotation

$$\tilde{\rho}_{mn}^\circledast = \sum_{b,d} e^{i\varphi(b-d)} d_{mb}^{(1)}(\vartheta) d_{dn}^{(1)}(\vartheta) \tilde{\rho}_{bd}^{(0)}, \quad (7)$$

where $d^{(1)}$ is the Wigner's (small) d-matrix of the first order [14]. To illustrate this, let us consider rotation of the system by $\vartheta = \pi/2$ and $\varphi = 0$, which allows to encode information about the $\Delta m = 1$ coherences in the detectable signal

$$\begin{aligned} \tilde{\rho}_{11}^\circledast - \tilde{\rho}_{-1-1}^\circledast &= \hat{\mathcal{D}}\left(0, \frac{\pi}{2}, 0\right) \tilde{\rho}^{(0)} \hat{\mathcal{D}}^\dagger\left(0, \frac{\pi}{2}, 0\right) = \\ &= -\frac{1}{\sqrt{2}} \left(\tilde{\rho}_{-10}^{(0)} + \tilde{\rho}_{0-1}^{(0)} + \tilde{\rho}_{10}^{(0)} + \tilde{\rho}_{01}^{(0)} \right). \end{aligned} \quad (8)$$

Similarly, it can be shown that the rotation of the state mixes the $\Delta m = 2$ coherences with population of the $m = 0$ sublevel, which eventually enables the full reconstruction of the ground-state density matrix.

Simulations – In order to test the developed quantum-state tomography protocol, we perform numerical simulations of a given-state density-matrix evolution. Based on numerical simulations, we determine the polarization rotation of x -polarized light, which is next contaminated with white noise and then used for reconstruction of the density matrix. The reconstruction is based on fitting the polarization-rotation signals $\Delta\alpha$ with

$$\Delta\alpha = e^{-\gamma t} [A_\alpha \sin(2\Omega_L t) + B_\alpha \cos(2\Omega_L t) + C_\alpha], \quad (9)$$

where A_α , B_α , and C_α are the fitting parameters. In our fitting routine, the three amplitudes are the only free parameters, i.e., the Larmor frequency Ω_L and the ground-state relaxation rate γ are known (the Larmor frequency Ω_L is known from the strength of the magnetic field applied during probing and the ground-state relaxation rate γ could be determined based on other measurements, such as relaxation in the dark [9, 19]). It should be noted that constraining Ω_L and γ allow extractions of A , B , and C even in the case of a poor signal-to-noise ratio (SNR).

Combining Eqs. (5), (7), and (9) allows derivation of the explicit relations between the fitting parameters and the post-pulse ground-state density-matrix elements

$$\tilde{\rho}_{1-1}^{\circlearrowleft} = (\tilde{\rho}_{-11}^{\circlearrowleft})^* = \frac{A_\alpha - iB_\alpha}{\zeta L}, \quad (10a)$$

$$\tilde{\rho}_{-1-1}^{\circlearrowleft} - \tilde{\rho}_{11}^{\circlearrowleft} = \frac{C_\alpha}{\zeta L}. \quad (10b)$$

As discussed above, a single fitting provides access to three density-matrix elements (compare with a technique describe, for example, in Ref. [7]). Other density-matrix elements can be acquired through appropriate choice of the magnetic-field pulses [Eq. (7)]. In a noiseless system, three sets of the pulses allow for full tomography of the $F = 1$ state. However, presence of noise and imperfections of the matrix manipulation (e.g., uncertainty of the pulse-rotation angles or Larmor-precession frequency) may introduce uncertainties in the reconstruction. This may lead to reconstruction of the matrix that does not correspond to a physical state. To accommodate for such an uncertainty, a larger set of pulses may be used but even then the results may be unphysical. To address this problem, many approaches can be implemented (see, for example, Ref. [20, 21]).

Our reconstruction protocol is based on the minimization of the distance between measured matrices and reconstructed matrix. For that we assume that distance between matrices is defined based on the Frobenius norm

$$\delta(\rho_r) = \sum_j \text{Tr} [(\rho_j - \rho_r)^\dagger \cdot (\rho_j - \rho_r)], \quad (11)$$

where ρ_j is j -th “measured” matrix. As the optimization with constraints of the semi-positivity and normalization tends to be computationally demanding and we want to

keep our algorithm as simple as possible, we first minimize the distance δ and then find a semi-positive matrix closest to the reconstructed one. To do so, we use the Frobenius-norm semi-positive approximant [22].

To demonstrate applicability of the technique, we first consider reconstruction of a pure state. The density matrix, corresponding to a nontrivial pure state, is shown in Fig. 1a) (blue bars). The signals [Figs. 1c-f)] were cal-

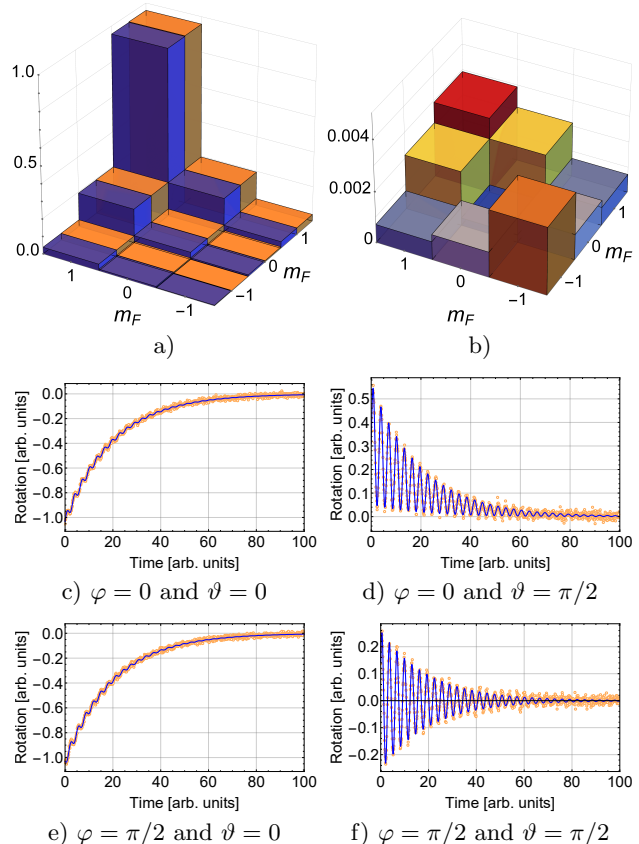


FIG. 1: (a) Magnitude of density-matrix elements of the reconstruction density matrix (blue) of a randomly chosen pure state (orange). (b) The difference between magnitudes of the density-matrix elements of the reconstructed and initial state. Simulated signals of polarization rotation for a set of initial magnetic-field pulses: (c) $\varphi = 0$ and $\vartheta = 0$, (d) $\varphi = 0$ and $\vartheta = \pi/2$, (e) $\varphi = \pi/2$ and $\vartheta = 0$, and (f) $\varphi = \pi/2$ and $\vartheta = \pi/2$. The simulations are performed in for the Larmor-frequency normalized set of parameters: $\Omega_R = 1$, $\Gamma = \Delta = 1000$, $\gamma = 0.05$ and $\Omega_R = 1$, $N_{at} = 10^{10}$, and $\Omega_L^{pulse} = 100$, $\Omega_L = 1$.

culated for a set of four arbitrarily chosen magnetic-field pulses. To mimic “experimental” data, we contaminate the simulated signals with white noise. To introduce a measure of the noise we define SNR as a ratio between amplitude of a signal measured for a fully aligned state (see SI) to root-mean-square of noise. In the considered

case, the generated signals were contaminated with noise of $\text{SNR} = 25$. Based on such noisy signals, the data were fitted and based on the fitting the density matrix was reconstructed [Fig. 1a), orange bars]. As shown in Fig. Fig. 1b), presenting the difference between assumed and reconstructed density matrix, the reconstruction is reliable. To quantify the performance of the protocol, we calculated the fidelity \mathcal{F}

$$\mathcal{F}(\rho_r, \rho') = \left(\text{Tr} \left[\sqrt{\sqrt{\rho_r} \rho^{(0)} \sqrt{\rho_r}} \right] \right)^2, \quad (12)$$

which, in the considered case, was 0.997.

Next, we analyzed the reconstruction of a partially mixed state (Fig. 2). Similarly, as before, the rotation

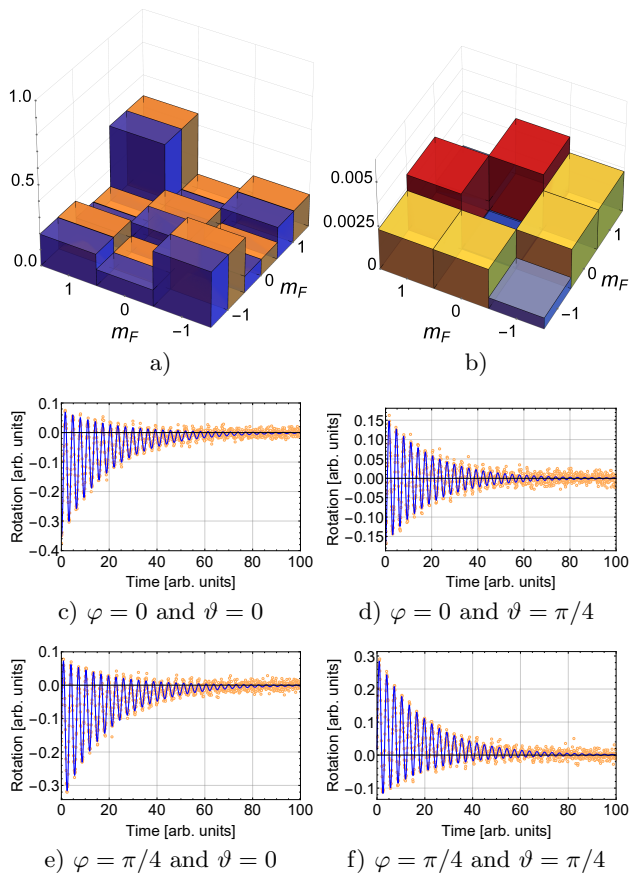


FIG. 2: Reconstruction of the partially mixed state: initial -orange and reconstructed - blue (a) state and absolute values of differences between matrices elements (b). The rotation signals, along with the fitting, for $\varphi = 0$ and $\theta = 0$ (c), $\varphi = 0$ and $\theta = \pi/4$ (d), $\varphi = \pi/4$ and $\theta = 0$ (e), and $\varphi = \pi/4$ and $\theta = \pi/4$ (f). The simulation parameters identical as in Fig. 1.

signals were simulated and white noise was added to the data. A noticeable difference between this and the previous result is the amplitude of the observed signals, being smaller for the mixed state. In fact, one can formulate

the general observation that the more mixed the state is, the lower the amplitudes of the signal one observes. The fitting for the signals allowed reconstruction of the density-matrix with the fidelity of 0.996.

An important question concerning the reconstruction is the role of SNR and uncertainty of the rotation pulses on the fidelity of the state reconstruction. To address this question, we analyze the fidelity of reconstruction of the pure states and fully mixed state (unpolarized state) versus SNR and uncertainty of the initial rotation (DC pulses). For each SNR or angle uncertainty, the reconstruction was performed 100 times with a set of four pulses rotating the matrix around z and y by random angles. The randomization of the rotation angles was introduced to avoid trapping of the reconstruction in local minima. Additionally, the fidelity of the reconstruction for the pure states was averaged over ten different pure states, which were obtained from the stretched state by a unitary evolutions, generated from the Haar measure [23].

To estimate average value and the variance of the fidelity, we plot the histograms of the achieved fidelities for every set of analyzed parameters and fit the beta distribution [24]. The choice of beta distribution was dictated by the fact that fidelity is limited to the range $[0, 1]$. Thus, the average values of fidelity and their error bars are given by expected value and variance of the beta distribution, respectively. The results, shown in Fig. 3, reveal that already with a single-set of four measurements, each with SNR at a level of 1, the fidelity exceeds 0.9 and at the level of 10, it is close to the unity. Somewhat

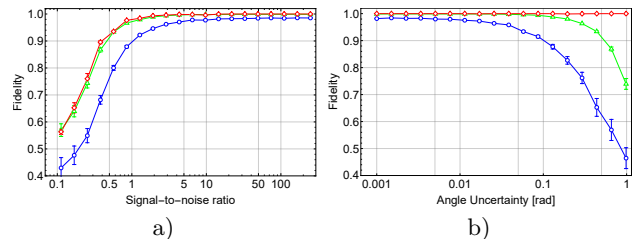


FIG. 3: Fidelity of the state reconstruction versus SNR (a) and uncertainty of the magnetic-field pulse rotation (b). The results are shown for a pure states (blue), partially mixed - purity ≈ 0.6 (green) and fully mixed state (red).

surprisingly event for an SNR below 1, the fidelity of the reconstruction is still decent, especially for partially mixed states. This originates from constraining the Larmor frequency Ω_L and relaxation/decay rate γ of the signal, which significantly limits the parameter space of the possible amplitudes A_α , B_α and C_α . Another question is the uncertainty of the rotation angle of the initial density matrix. With the simulations, we showed that all the way up to several tens of milliradians, uncertainty in the rotation has almost no effect on the fidelity of the

reconstruction. For larger uncertainty, the fidelity starts to deteriorate (with a distinct exception of the thermal state, which is fully isotropic). Nonetheless, the precision of the rotation at the level of a few degree, which is easily experimentally achievable, ensures the good reconstruction of the state.

From the perspective of practical implementation of the protocol [25], an important question concerns the number of measurements needed for reliable reconstruction of the quantum state. Generally, in our system, one needs to measure at least three polarization-rotation signals to fully reconstruct the density matrix. However, as shown in Fig. 4a), for even lower number of measurements, the partial reconstruction is possible, though fidelity of the reconstruction is small. In principle, the

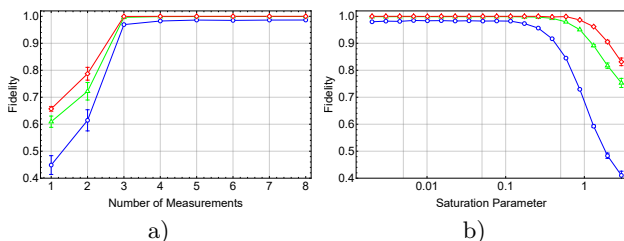


FIG. 4: Fidelity of the reconstruction versus (a) number of measurements and (b) strength of the light-matter coupling, expressed as the saturation constant κ_2 , for pure (blue), mixed (green), and thermal (red) states.

The calculations were performed for the parameters same as in Fig. 3 with $\text{SNR} \approx 25$ and no uncertainty in the rotation.

higher the number of measurements, the more precise the reconstruction is. This becomes particularly important in noisy media, where low signal quality needs to be overcome by more measurements, so that the minimization, being the last stage of the algorithm, can be performed more precisely.

Different contribution to the uncertainty of the reconstruction comes from the action of the probing beam. For the considerations, we have assumed that the action of probe light is so small that it negligible. Generally, this is not true and the probe action can manifest at various levels. For instance, even in a simple case of classical light, there is nonzero probability of the optical excitation by an off-resonant (probe) beam. This manifests as optical pumping, which modifies the reconstructed state and hence decreases the fidelity of the reconstruction. This effect is shown in Fig. 4b), where fidelity is measured versus the probe-light saturation parameter $\kappa_2 = \Omega_R^2/(\Gamma\gamma)$ [17]. For small κ_2 , the pumping is inefficient so the probe light does not affect the state, however, the higher the probe-light intensity, the more probable the excitation, which deteriorates the fidelity of the reconstruction. This effect is reduced in paraffin-coated cells, where atoms, freely moving across the cell

and getting in and out of the light beam, effectively average the perturbation across the whole cell [8]. It allows to achieve the effective saturation parameter roughly two orders of magnitude smaller than in cold atomic ensemble [8].

Conclusions – In this work, we presented the protocol of the reconstruction of the collective density matrix of the $F = 1$ ground state of atoms under the action of linearly polarized light and DC magnetic field. By deriving explicit relation between polarization rotation/ellipticity change and ground-state density-matrix elements, we demonstrate the ability of the full reconstruction of the state. The fidelity of the reconstruction was examined against such factors as noise, experimental uncertainties, and number of measurements, demonstrating robustness of the technique against these factors.

Our technique can be implemented in experimental investigations [25]. In particular, we plan to use it for reconstruction of a collective quantum state of the $F = 1$ state of room-temperature ^{87}Rb vapor contained in a paraffin-coated cell. By observation of polarization rotation of linearly polarized off-resonant light, we plan to reconstruct the state initially generated and modified using sequences of light pulses, as well as static and oscillating magnetic fields.

We also plan to generalize the technique to accommodate for systems with larger F . It will require addressing several issues, particular, differentiating signals originating from different ground-state coherences. We plan to approach this problem, and lift degeneracy of different-coherence contributions either by implementation of non-linear Zeeman effect [26] or AC Stark effect [7]. Implementation of the approach should allow for thorough reconstruction of such a ground state, particularly make possible detection of both hyperfine states of rubidium atoms.

-
- [1] M. Paris and J. Rehacek, eds., *Quantum State Estimation*, Vol. 649 (Springer, Berlin, Heidelberg, 2004).
 - [2] Y. Liu, J. Tian, R. Betzholtz, and J. Cai, “Pulsed Quantum-State Reconstruction of Dark Systems,” *Phys. Rev. Lett.* **122**, 110406 (2019).
 - [3] S. Mancini and P. Tombesi, “Quantum state reconstruction of a bose-einstein condensate,” *EPL* **40**, 351–356 (1997).
 - [4] H. J. Briegel, D. E. Browne, W. Dür, R. Raussendorf, and M. Van den Nest, “Measurement-based quantum computation,” *Nature Physics* **5**, 19–26 (2009).
 - [5] J. I. Cirac, L.-M. Duan, D. Jaksch, and P. Zoller, “Quantum Information Processing with Quantum Optics,” in *International Conference on Theoretical Physics*, edited by Daniel Iagolnitzer, Vincent Rivasseau, and Jean Zinn-Justin (Birkhäuser Basel, Basel, 2004) pp. 759–781.
 - [6] W. K. Wootters and W. H. Zurek, “A single quantum

- cannot be cloned,” *Nature* **299**, 802–803 (1982).
- [7] I. H. Deutsch and P. S. Jessen, “Quantum control and measurement of atomic spins in polarization spectroscopy,” *Opt. Commun.* **283**, 681–694 (2010).
- [8] E. Zhivun, A. Wickenbrock, J. Sudyka, B. Patton, S. Pustelny, and D. Budker, “Vector light shift averaging in paraffin-coated alkali vapor cells,” *Opt. Express* **24**, 15383–15390 (2016).
- [9] M. T. Graf, D. F. Kimball, S. M. Rochester, K. Kerner, C. Wong, D. Budker, E. B. Alexandrov, M. V. Balabas, and V. V. Yashchuk, “Relaxation of atomic polarization in paraffin-coated cesium vapor cells,” *Phys. Rev. A* **72**, 23401 (2005).
- [10] M. V. Balabas, T. Karaulanov, M. P. Ledbetter, and D. Budker, “Polarized Alkali-Metal Vapor with Minute-Long Transverse Spin-Relaxation Time,” *Phys. Rev. Lett.* **105**, 70801 (2010).
- [11] V. G. Lucivero, R. Jiménez-Martínez, J. Kong, and M. W. Mitchell, “Squeezed-light spin noise spectroscopy,” *Phys. Rev. A* **93**, 53802 (2016).
- [12] V. G. Lucivero, P. Anielski, W. Gawlik, and M. W. Mitchell, “Shot-noise-limited magnetometer with sub-picotesla sensitivity at room temperature,” *Rev. Sci. Instrum.* **85**, 113108 (2014).
- [13] B. Julsgaard, A. Kozhekin, and E. S. Polzik, “Experimental long-lived entanglement of two macroscopic objects,” *Nature* **413**, 400–403 (2001).
- [14] J. J. Sakurai and J. Napolitano, *Modern Quantum Mechanics* (Cambridge University Press, 2017).
- [15] G. A. Smith, S. Chaudhury, A. Silberfarb, I. H. Deutsch, and P. S. Jessen, “Continuous weak measurement and nonlinear dynamics in a cold spin ensemble,” *Phys. Rev. Lett.* **93**, 163602 (2004).
- [16] S. Pustelny, D. F. Jackson Kimball, S. M. Rochester, V. V. Yashchuk, W. Gawlik, and D. Budker, “Pump-probe nonlinear magneto-optical rotation with frequency-modulated light,” *Phys. Rev. A* **73**, 23817 (2006).
- [17] M. Auzinsh, D. Budker, and S. Rochester, *Optically Polarized Atoms: Understanding Light-atom Interactions* (OUP Oxford, 2010).
- [18] D. Budker, L. Hollberg, D. F. Kimball, J. Kitching, S. Pustelny, and V. V. Yashchuk, “Microwave transitions and nonlinear magneto-optical rotation in anti-relaxation-coated cells,” *Phys. Rev. A* **71**, 012903 (2005).
- [19] W. Chalupczak, P. Josephs-Franks, R. M. Godun, and S. Pustelny, “Radio-frequency spectroscopy in the dark,” *Phys. Rev. A* **88**, 052508 (2013).
- [20] E. Bagan, A. Monras, and R. Muñoz-Tapia, “Comprehensive analysis of quantum pure-state estimation for two-level systems,” *Phys. Rev. A* **71**, 062318 (2005).
- [21] R. Schmied, “Quantum state tomography of a single qubit: comparison of methods,” *J. Mod. Phys.* **63**, 1744–1758 (2016).
- [22] N. J. Higham, “Computing a nearest symmetric positive semidefinite matrix,” *Linear Algebra and its Applications* **103**, 103–118 (1988).
- [23] K. Życzkowski, K. A. Penson, I. Nechita, and B. Collins, “Generating random density matrices,” *Journal of Mathematical Physics* **52**, 62201 (2011).
- [24] M. Enríquez, F. Delgado, and K. Życzkowski, “Entanglement of Three-Qubit Random Pure States,” *Entropy* **20** (2018), 10.3390/e20100745.
- [25] F. Juras, M. Kopciuch, and S. Pustelny, “Tutaj trzeba wymyślić jakiś tytuł,” In preparation.
- [26] S. Pustelny, M. Koczwarą, L. Cincio, and W. Gawlik, “Tailoring quantum superpositions with linearly polarized amplitude-modulated light,” *Phys. Rev. A* **83**, 043832 (2011).

Optical reconstruction of collective density matrix of qutrit Supplemental Information

Marek Kopciuch¹ and Szymon Pustelny¹

¹*Institute of Physics, Jagiellonian University in Kraków, Łojasiewicza 11, 30-348 Kraków, Poland*

(Dated: March 21, 2022)

DERIVATION OF RELATIONS

General theoretical treatment of light propagation through atomic ensemble

In semi-classical approximation, the relation between light and atomic properties is governed by the Maxwell equation [1]:

$$\nabla^2 \mathbf{E} - \frac{1}{c^2} \partial_t^2 \mathbf{E} = \mu_0 \partial_t^2 \mathbf{P}, \quad (1)$$

where \mathbf{E} is the electric field of light and \mathbf{P} is the polarization of atoms. Taking a generic form of light

$$\mathbf{E} = E_0 \text{Re} \left\{ e^{i(kz - \omega t + \phi)} \left(\cos(\epsilon) [\cos(\alpha) \mathbf{x} + \sin(\alpha) \mathbf{y}] + i \sin(\epsilon) [\cos(\alpha) \mathbf{y} - \sin(\alpha) \mathbf{x}] \right) \right\}, \quad (2)$$

where E_0 , ϕ , ϵ , α , ω and k are amplitude, phase, ellipticity, polarization rotation, frequency and wavenumber of light, respectively, and assuming the polarization can be written as

$$\mathbf{P} = \text{Re} \left\{ e^{i(kz - \omega t + \phi)} \left[(P_1 - i P_2) \mathbf{x} + (P_3 - i P_4) \mathbf{y} \right] \right\}, \quad (3)$$

where P_i are respective quadrature components of the polarization, allow derivation of an explicit relation between specific properties of light and given polarization quadratures. In particular, substituting Eqs. (2) and (3) into Eq. (1) and neglecting the second-order derivatives enable to derive relations for polarization rotation and degree of ellipticity on the quadratures P_i . Taking linearly polarized light ($\epsilon = 0$), the polarization rotation and ellipticity change, defined as a partial derivative over distance, are given by

$$\partial_z \alpha = \frac{\omega}{2\epsilon_0 E_0 c} [\cos(\alpha) P_4 - \sin(\alpha) P_2], \quad (4a)$$

$$\partial_z \epsilon = \frac{\omega}{2\epsilon_0 E_0 c} [-\sin(\alpha) P_1 + \cos(\alpha) P_3]. \quad (4b)$$

$$\mathbf{P} = N_{at} \langle \hat{\mathbf{d}} \rangle = N_{at} \text{Tr} [\rho \hat{\mathbf{d}}], \quad (5)$$

where ρ is the density matrix, N_{at} is the atomic number density and, $\langle \hat{\mathbf{d}} \rangle$ denotes the expectation value. To present the polarization \mathbf{P} given by Eq. (5) in a form similar to that of Eq. (3), the density matrix ρ needs to be transform to the frame rotating at the light frequency ω

$$\rho = U \tilde{\rho} U^\dagger = \begin{pmatrix} (\tilde{\rho}_{ij}) & (\tilde{\rho}_{ij'}) e^{i\omega t} \\ (\tilde{\rho}_{i'j}) e^{-i\omega t} & (\tilde{\rho}_{i'j'}) \end{pmatrix}, \quad (6)$$

where $(\tilde{\rho}_{ij})$ and $(\tilde{\rho}_{i'j'})$ are the submatrices corresponding to the ground and excited states and $(\tilde{\rho}_{i0'})$ denotes the submatrix describing the optical coherences between the states, with $\tilde{\rho}_{ij}$ ($\tilde{\rho}_{i'j'}$) being the density-matrix elements between the i and j (i' and j') ground-state (excited-state) sublevels, $\tilde{\rho}_{ij'}$ the amplitudes of the optical coherence between the ground state i and the excited state j' , and $\rho_{i''}$ the excited-state population. The rotation transformation

is given by $U = \text{diag}(1, \dots, 1, e^{-i\omega t}, \dots, e^{-i\omega t})$, where number of elements by 1 and $e^{-i\omega t}$ is determined by the degeneracy of the ground and excited state, respectively.

Let us now focus on a specific example of an $F = 1 \rightarrow F' = 0$ system considered within this work. In such a case, tracing over Eq. (5) returns

$$\mathbf{P} = N_{at} \text{Re} \left\{ \sqrt{\frac{2}{3}} \langle 1 \| \hat{\mathbf{d}}^{(F)} \| 0 \rangle e^{-i\omega t} \left[(\tilde{\rho}_{0'-1} - \tilde{\rho}_{0'1}) \mathbf{x} + i(\tilde{\rho}_{0'-1} + \tilde{\rho}_{0'1}) \mathbf{y} + \sqrt{2} \tilde{\rho}_{0'0} \mathbf{z} \right] \right\}. \quad (7)$$

where $\langle 1 \| \hat{\mathbf{d}}^{(F)} \| 0 \rangle$ indicates the reduced dipole moment in hyperfine coupling and the Wigner-Eckart theorem follows the convention of Ref. [2]. If one assumes that light propagates along z , the last term in square brackets disappears, which allows to rewrite Eqs. (4) into

$$\partial_z \alpha = \chi \left[-\sin(\alpha) \text{Im} \{ \tilde{\rho}_{0'-1} - \tilde{\rho}_{0'1} \} - \cos(\alpha) \text{Re} \{ \tilde{\rho}_{0'-1} + \tilde{\rho}_{0'1} \} \right], \quad (8a)$$

$$\partial_z \epsilon = \chi \left[-\sin(\alpha) \text{Re} \{ \tilde{\rho}_{0'-1} - \tilde{\rho}_{0'1} \} + \cos(\alpha) \text{Im} \{ \tilde{\rho}_{0'-1} + \tilde{\rho}_{0'1} \} \right], \quad (8b)$$

where $\chi = \omega N_{at} \langle 1 \| \hat{\mathbf{d}}^{(F)} \| 0 \rangle / (\sqrt{6} \epsilon_0 E_0 c)$. To simplify the relation, we can use the identity (see, for example, Ref. [2])

$$\langle J_g I F_g \| \hat{\mathbf{d}}^{(F)} \| J_e I F_e \rangle = (-1)^{J_g + I + F_e + 1} \langle J_g \| \hat{\mathbf{d}}^{(J)} \| J_e \rangle \sqrt{(2F_g + 1)(2F_e + 1)} \begin{Bmatrix} J_g & F_g & I \\ F_e & J_e & 1 \end{Bmatrix} \quad (9)$$

and the relation

$$\Gamma = \frac{\omega_0^3}{3\pi\epsilon_0 \hbar c^3} \frac{|\langle J_g \| \hat{\mathbf{d}}^{(J)} \| J_e \rangle|^2}{2J_e + 1}, \quad (10)$$

where $\Omega_R = \langle 1 \| \hat{\mathbf{d}}^{(F)} \cdot \mathbf{E} \| 0 \rangle / \hbar$ is the Rabi frequency and $J_g = 1$ i $J_e = I = 0$ allows to present χ as

$$\chi = \frac{3\pi}{\sqrt{2}} \frac{\omega}{\omega_0} \frac{N_{at} \Gamma}{\Omega_R} \left(\frac{\hbar c}{\omega_0} \right)^2 \approx \frac{3\pi}{\sqrt{2}} \frac{N_{at} \Gamma}{\Omega_R} \left(\frac{\hbar c}{\omega_0} \right)^2. \quad (11)$$

Density-matrix evolution

Quantum-mechanical evolution of a quantum state, described using the density matrix, can be calculated using the Liouville equation

$$\frac{d}{dt} \rho = \frac{1}{i\hbar} [\hat{H}, \rho] - \{\hat{\Gamma}, \rho\} + \hat{\Lambda}(\rho), \quad (12)$$

where \hat{H} is the total Hamiltonian of the system and $\hat{\Gamma}$ and $\hat{\Lambda}$ are relaxation operators responsible for relaxation and repopulation of the levels (see, for example, Ref. [1]). The Hamiltonian \hat{H} is a sum of unperturbed Hamiltonian \hat{H}_0 and the interaction operator \hat{V} , which, in the considered case, accounts for interaction with light and magnetic field

$$\hat{H} = \hat{H}_0 + \hat{V} = \hat{H}_0 - \mathbf{E} \cdot \hat{\mathbf{d}} - \mathbf{B} \cdot \hat{\boldsymbol{\mu}}, \quad (13)$$

where $\hat{\boldsymbol{\mu}}$ is the magnetic moment operator and \mathbf{B} denotes the magnetic field. Substituting Eq. (13) into Eq. (12) allows one to calculate the evolution of specific density-matrix elements. To separate the fast (oscillating at the optical frequency) evolution of the system, the density matrix is transformed using the rotating-wave approximation.

Let us now consider a system subjected to the static magnetic field $\mathbf{B} = \mathbf{z}B_0$, corresponding to the Larmor frequency $\Omega_L = g_F \mu_B B / \hbar$, with g_F being the Landé factor and μ_B the Bohr magneton, interacting with x -polarized light. Substituting these parameters into Eq. (13) and next into Eq. (12) allows us to calculate amplitude of the optical coherences generated by the light

$$\frac{d}{dt} \tilde{\rho}_{-10'} = \tilde{\rho}_{-10'} \left[-\frac{2\gamma + \Gamma}{2} - i(\Delta - \Omega_L) \right] - \frac{i\Omega_R}{2\sqrt{6}} (-\tilde{\rho}_{0'0'} + \tilde{\rho}_{-1-1} - \tilde{\rho}_{-11}), \quad (14a)$$

$$\frac{d}{dt} \tilde{\rho}_{10'} = \tilde{\rho}_{10'} \left[-\frac{2\gamma + \Gamma}{2} - i(\Delta + \Omega_L) \right] - \frac{i\Omega_R}{2\sqrt{6}} (\tilde{\rho}_{0'0'} - \tilde{\rho}_{11} + \tilde{\rho}_{1-1}), \quad (14b)$$

where γ and Γ are the ground- and excited-state relaxation rates, respectively and $\Delta = \omega - \omega_0$ is the detuning of light from an optical transition. A similar substitution may be used to calculate the ground-state density-matrix elements yielding

$$\frac{d}{dt}\tilde{\rho}_{11} = \gamma \left(-\tilde{\rho}_{11} + \frac{1}{3} \right) + \frac{\Gamma}{3}\tilde{\rho}_{0'0'} - \frac{\Omega_R}{2\sqrt{6}}(\tilde{\rho}_{10'} + \tilde{\rho}_{0'1}), \quad (15a)$$

$$\frac{d}{dt}\tilde{\rho}_{-1-1} = \gamma \left(-\tilde{\rho}_{-1-1} + \frac{1}{3} \right) + \frac{\Gamma}{3}\tilde{\rho}_{0'0'} - \frac{\Omega_R}{2\sqrt{6}}(\tilde{\rho}_{-10'} + \tilde{\rho}_{0'-1}), \quad (15b)$$

$$\frac{d}{dt}\tilde{\rho}_{-11} = (-\gamma + 2i\Omega_L)\tilde{\rho}_{-11} - \frac{\Omega_R}{2\sqrt{6}}(\tilde{\rho}_{-10'} + \tilde{\rho}_{0'1}). \quad (15c)$$

Using Eqs. (14) and (15) one can calculate evolution of the density matrix. In our calculations, the equations were solved numerically, assuming the initial state $\rho^{(0)}$, being the state to be reconstructed. Based on the calculations and Eqs. (8), one can calculate time-dependent polarization rotation and ellipticity change, which are finally used for the quantum-state reconstruction.

RECONSTRUCTION OF SPECIFIC STATES

While the main text presents reconstruction of two generic cases, corresponding to arbitrary pure and mixed states, here we present results of the reconstructions of several simple but often experimentally generated, states [3–5].

The simplest state one may consider for reconstruction is a totally mixed state, corresponding to atoms in thermal equilibrium. In such a case, all ground-state population are equal and no coherences are present in the system. It can be shown, using the atomic density-matrix probability surfaces [6], that this state is perfectly symmetric, and hence no polarization rotation or ellipticity change is expected. We also expect that due to full symmetry of the density matrix, its observation from different directions also provides the same zero outcome. It should be noted, however, in the real measurement, the signal is contaminated with noise or systematic effects, associated with imperfections of detection, which can lead to nonzero results.

The results of the simulations of the polarization rotation proceeded with pulses rotating density matrix by the angle φ and θ are shown in Fig. 1c)-f). In order to better simulate the experimental signals, the simulated data was superimposed with white noise and next they were used to reconstruct the density matrix by fitting the experimental data (blue traces at experimental data). Figure 1a) shows initial and reconstructed density matrix. Under such conditions, fidelity of the reconstruction is very close to unity $\mathcal{F} = 0.999$. Figure 1b) presents deviation of the reconstructed matrix from the initial matrix, At this level it is hard to determine whether this deviations are a consequence of the principal uncertainty of our method resulting from the approximations in the model or fitting errors (we can clearly see oscillations of fitting function at the beginning of the signal in Fig. 1c)-f), while such behaviour is not being expected).

An aligned state is a non-trivial state that is generated by linearly polarized (here, x -polarized) light. Such a state is widely used in optical magnetometry [7–10]. Characteristic feature of that state is the presence of a strong $\Delta m = 2$ coherence with simultaneous absence of $\Delta m = 1$ coherences. The density matrix corresponding to such a state is shown in Fig. 2a) with an initial state shown in orange and reconstructed state in blue. Based on the geometric argument using the probability surface [1, 6] (the density matrix corresponds to the peanut-like shape oriented along the polarization direction), rotation around the magnetic field perpendicular to the axis of the peanut yields a two-fold symmetry. Hence the rotation signal around such a field lead to appearance of polarization rotation modulated at twice the Larmor frequency. At the same time, rotation and differently oriented fields gives the signals both at the first and second harmonic of the Larmor frequency [11], with a distinct exception of rotation around the peanut axis which provides no modulation (full symmetry around the axis). The simulated signals (with noise added) along with the fitting functions are shown in Fig. 2c)-f). Based on the signals, we performed the reconstruction and achieved a fidelity of 0.998.

The second, non-trivial state, often encountered experimentally, is the fully oriented state (the stretch state). This state is generated by circularly polarized light, which pumps atoms into the ground-state sublevel of a maximum or minimum magnetic number m . The corresponding density matrix is shown in Fig. 3a). The geometrical analysis of the state, based on the probability surface shows that when oriented along the magnetic field, there is no precession signal. However, because of the relaxation processes, the system returns into the polarization equilibrium, and the population misbalance between the $m = -1$ and $m = 1$ sublevels disappears. As discussed in the main text, the population misbalance results in static rotation, we one expects nonzero nonoscillating rotation, which decays over time. Indeed, such a behavior is observed in two of the data sets, corresponding to $\varphi = 0$, $\theta = 0$ and $\varphi = \pi/2$, $\theta = 0$

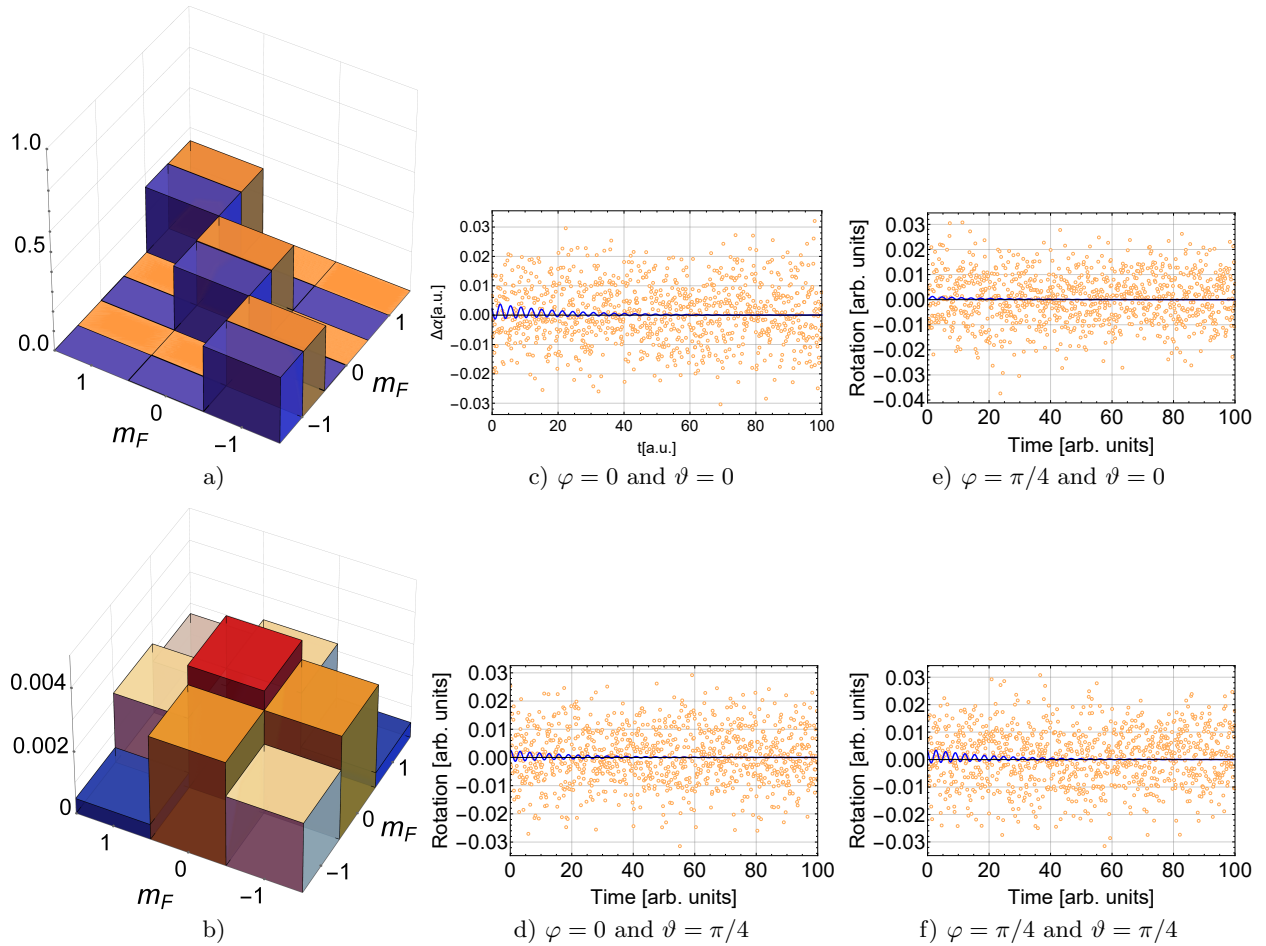


FIG. 1: Reconstruction of the totally mixed state. (a) Absolute values of density-matrix elements corresponding to initial (orange) and reconstructed (blue) states and (b) the absolute differences between the density matrices. The rotation signals (orange points) along with the fitting (blue line) for c) $\varphi = 0$ and $\vartheta = 0$, d) $\varphi = 0$ and $\vartheta = \pi/4$, e) $\varphi = \pi/4$ and $\vartheta = 0$, and f) $\varphi = \pi/4$ and $\vartheta = \pi/4$. Simulation parameters identical as in the main text.

pulse sets. However, when the shape is oriented at an angle to the magnetic field, it provides an oscillating signal which is also visible in the simulations. Based on the simulations [Fig. 3c-f)], the density matrix was reconstructed [blue bars in Fig. 3a)]. The differences between the initial and reconstructed matrix are shown in Fig. 3b) and the fidelity of the reconstruction equals 0.999.

These three representative examples form a basis, which allows to build most of the states. This demonstrates the capability of the reconstruction of an arbitrary quantum state in the $F = 1$ ground state of atoms interacting with light.

-
- [1] M. Auzinsh, D. Budker, and S. Rochester, *Optically Polarized Atoms: Understanding Light-atom Interactions* (OUP Oxford, 2010).
 - [2] I. I. Sobelman, *Atomic Spectra and Radiative Transitions*, Springer Series in Chemical Physics (Springer-Verlag Berlin Heidelberg, 1979).
 - [3] W. Gawlik, L. Krzemień, S. Pustelny, D Sangla, J. Zachorowski, M. Graf, A. O. Sushkov, and D. Budker, “Nonlinear magneto-optical rotation with amplitude modulated light,” *Appl. Phys. Lett.* **88**, 131108 (2006).
 - [4] S. Pustelny, D. F. Jackson Kimball, S. M. Rochester, V. V. Yashchuk, W. Gawlik, and D. Budker, “Pump-probe nonlinear magneto-optical rotation with frequency-modulated light,” *Phys. Rev. A* **73**, 23817 (2006).
 - [5] O. Katz and O. Firstenberg, “Light storage for one second in room-temperature alkali vapor,” *Nat. Commun.* **9**, 2074 (2018).

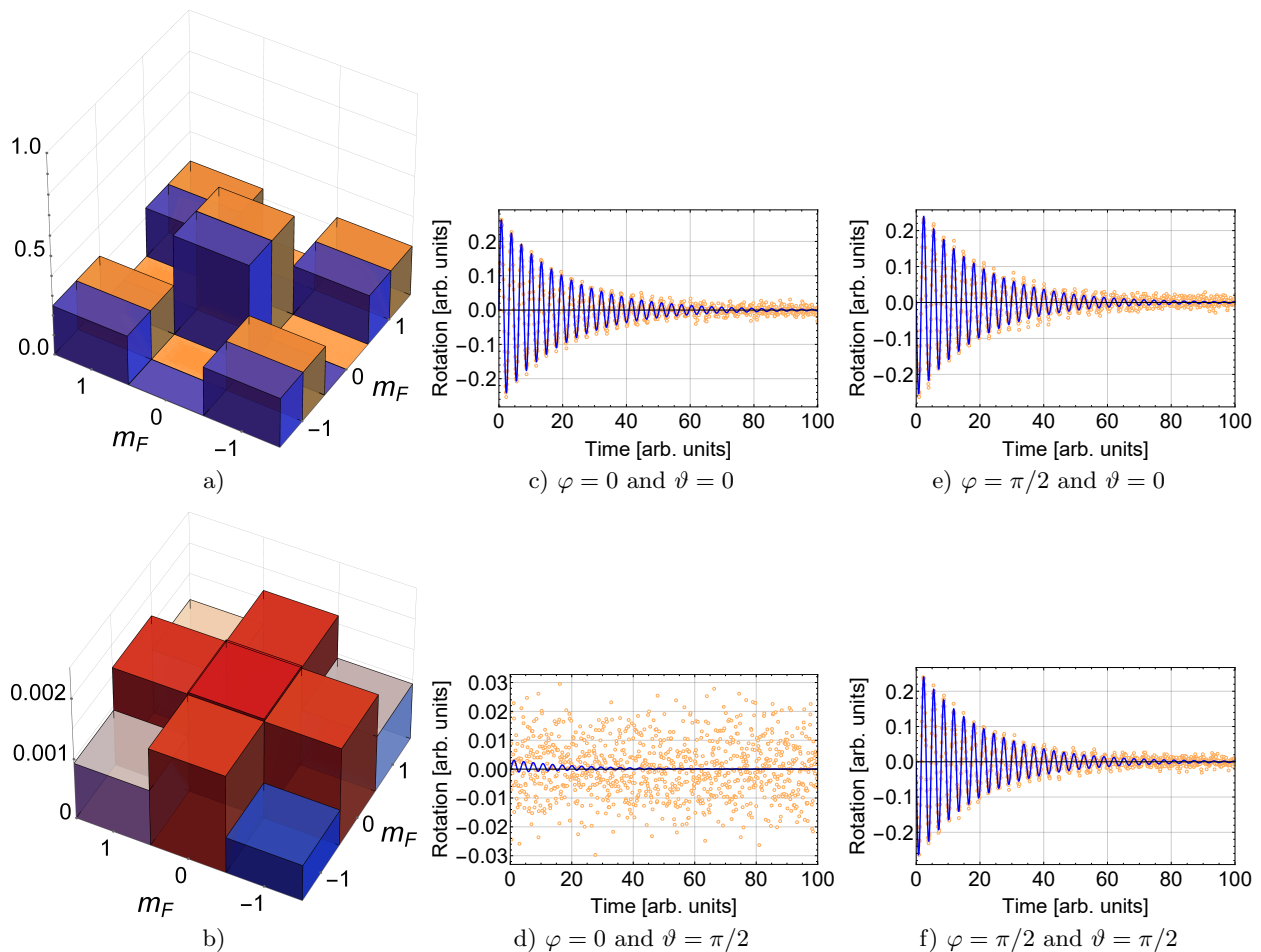


FIG. 2: Reconstruction of the density matrix of a fully aligned state. (a) Absolute values of the density-matrix elements corresponding to initial (orange) and reconstructed (blue) states with (b) the absolute value of the differences between the two matrices. c)-f) Simulated signals of polarization rotation obtained with pulse sequences same as in Fig. 1.

- [6] S. M. Rochester and D. Budker, “Atomic polarization visualized,” *Amer. J. Phys.* **69**, 450–454 (2001).
- [7] S. Pustelny, A. Wojciechowski, M. Gring, M. Kotyrba, J. Zachorowski, and W. Gawlik, “Magnetometry based on nonlinear magneto-optical rotation with amplitude-modulated light,” *J. Appl. Phys.* **103** (2008).
- [8] W. Chalupczak, P. Josephs-Franks, R. M. Godun, and S. Pustelny, “Radio-frequency spectroscopy in the dark,” *Phys. Rev. A* **88**, 052508 (2013).
- [9] Z. Ding, X. Long, J. Yuan, Z. Fan, and H. Luo, “Sensitive determination of the spin polarization of optically pumped alkali-metal atoms using near-resonant light,” *Sci. Rep.* **6** (2016).
- [10] N. Wilson, C. Perrella, R. Anderson, A. Luiten, and P. Light, “Wide-bandwidth atomic magnetometry via instantaneous-phase retrieval,” *Phys. Rev. Res.* **2** (2020).
- [11] S. Pustelny, W. Gawlik, S. M. Rochester, D. F. Jackson Kimball, V. V. Yashchuk, and D. Budker, “Nonlinear magneto-optical rotation with modulated light in tilted magnetic fields,” *Phys. Rev. A* **74**, 063420 (2006).

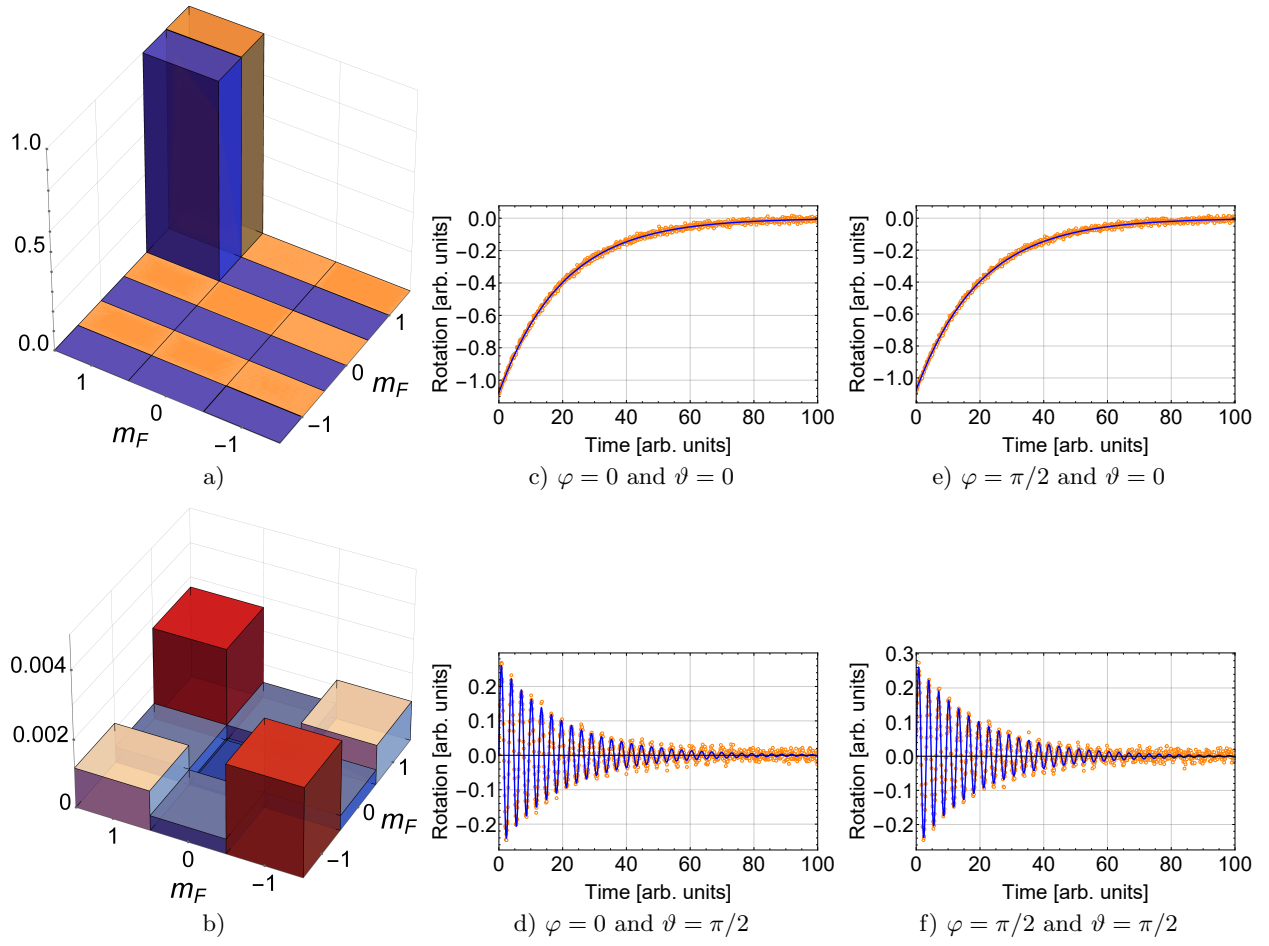


FIG. 3: Reconstruction of the density matrix corresponding to the stretch state. (a) Absolute value of the density-matrix elements of the initial (orange) and reconstructed (blue) states with (b) an absolute value of the differences between corresponding density-matrix elements. Simulated rotation signals obtained with a set of four initial DC magnetic field pulses. The pulse sequences are the same as in Fig. 1